



Research paper

# Modelling of a tubular membrane contactor for pre-combustion CO<sub>2</sub> capture using ionic liquids: Influence of the membrane configuration, absorbent properties and operation parameters

Zhongde Dai, Muhammad Usman, Magne Hillestad, Liyuan Deng\*

*Department of Chemical Engineering, Norwegian University of Science and Technology (NTNU), Trondheim, 7491, Norway*

Received 2 September 2016; revised 17 November 2016; accepted 18 November 2016

Available online 3 December 2016

## Abstract

A membrane contactor using ionic liquids (ILs) as solvent for pre-combustion capture CO<sub>2</sub> at elevated temperature (303–393 K) and pressure (20 bar) has been studied using mathematic model in the present work. A comprehensive two-dimensional (2D) mass-transfer model was developed based on finite element method. The effects of liquid properties, membrane configurations, as well as operation parameters on the CO<sub>2</sub> removal efficiency were systematically studied. The simulation results show that CO<sub>2</sub> can be effectively removed in this process. In addition, it is found that the liquid phase mass transfer dominated the overall mass transfer. Membranes with high porosity and small thickness could apparently reduce the membrane resistance and thus increase the separation efficiency. On the other hand, the membrane diameter and membrane length have a relatively small influence on separation performance within the operation range.

© 2016, Institute of Process Engineering, Chinese Academy of Sciences. Publishing services by Elsevier B.V. on behalf of KeAi Communications Co., Ltd. This is an open access article under the CC BY-NC-ND license (<http://creativecommons.org/licenses/by-nc-nd/4.0/>).

*Keywords:* CO<sub>2</sub> capture; Pre-combustion; Membrane contactor; Ionic liquids; Modelling

## 1. Introduction

Over the past few decades, the strong anthropogenic increase in the emission of greenhouse gases (primarily CO<sub>2</sub>) leads to global warming and climate change, which is one of the main growing issues our society has to face [1]. Large efforts have been carried out to reduce CO<sub>2</sub> emissions through a carbon capture and sequestration (CCS) process.

Generally, there are three different strategies for CO<sub>2</sub> capture, namely post-combustion, pre-combustion and oxy-fuel combustion. Particularly, Pre-combustion targets on separation of CO<sub>2</sub> from the synthesis gas (mixture of H<sub>2</sub> and CO<sub>2</sub>). Due to the concentrated CO<sub>2</sub> (45%) at high pressure and temperature, which can provide higher driving force for

separation, the pre-combustion CO<sub>2</sub> capture is considered as a relatively cheaper strategy with high plant efficiency [2–4]. Various technologies have been reported to separate CO<sub>2</sub> from syngas, including membranes, adsorption, absorption, chemical looping, and gas hydration. CO<sub>2</sub> capture from syngas using membrane contactors are rarely reported in the literature [5].

Membrane contactor is a hybrid technology combines the advantages of membrane and absorption. Compared to the conventional packed column for CO<sub>2</sub> absorption/stripping, it has advantages including larger interfacial area per unit volume, independent control of gas and liquid flow rates, small equipment size and lower operation cost [6,7]. Additionally, it avoids the problems often confronted in the conventional absorption equipment such as flooding, loading, weeping and foaming [8]. Various aqueous absorbent have been investigated in membrane contactors for CO<sub>2</sub> capture, such as aqueous amine solutions [9,10], amino acid salts solutions [11,12], alkaline solutions [13,14], enzyme solutions [15] and

\* Corresponding author.

E-mail address: [deng@ntnu.no](mailto:deng@ntnu.no) (L. Deng).

ammonia solutions [16]. However, up to now, only limited number of literature have been reported for CO<sub>2</sub> separation using membrane contactor with ionic liquids (ILs) as absorbent [5,17–22]. 1-ethyl-3-methylimidazolium ethylsulfate [Emim][Tf<sub>2</sub>N] was employed to capture CO<sub>2</sub> and SO<sub>2</sub> from flue gas using both parallel and cross-flow membrane contactors [22,23], while 1-butyl-3-methylimidazolium tricyanomethanide [Bmim][TCM] was used in both polymeric and inorganic membrane contactors for pre-combustion CO<sub>2</sub> capture [20,21].

Ionic liquids, with their distinctive properties such as negligible volatility, wide liquid regions, superior thermal stability, and tailorable structure, have been a hot research topic in both academic research and industrial applications in the past few decades [24,25]. Specifically, different kinds of ILs have been combined with membrane technology and used for CO<sub>2</sub> capture in the last decade, such as in the forms of supported ionic liquid membranes (SILMs) and poly-ionic liquid membranes [26–32].

Compared with traditional solvents used in membrane contactor, the ILs offer not only better thermal stability, which ensure the higher temperature application, but also lower volatility, which leads to lower solvent loss and lower regeneration energy consumption.

A membrane contactor process with closed cycle and continues flow using ILs as absorbent has been developed for pre-combustion CO<sub>2</sub> capture in our group [20] (Fig. 1). Different from the PSMAB process (pressure swing membrane absorption process) reported by Chau et al. [33], which is more like a traditional pressure swing adsorption process with the absorbent fixed in the membrane contactor, the continuous flow in this design is more efficient and easier to control.

Simulation is a powerful tool to reduce the cost of optimization of an available design and/or new design even at lab scale. Thus far, many researchers have simulated the membrane contactor systems for post-combustion [10,34–40], natural gas sweetening [41,42] and biogas upgrading [43,44]. But to the best of the authors' knowledge, there is no report on simulation

of membrane contactor for pre-combustion CO<sub>2</sub> capture using ILs as absorbent at elevated temperature and pressures. For the purpose of gaining an improved understanding and facilitating the optimization of CO<sub>2</sub> separation from syngas using membrane contactor and ILs, a simulation work is necessary.

In the present work, a comprehensive two-dimensional (2D) mass-transfer model was developed in Multiphysics COMSOL to simulate the CO<sub>2</sub> separation behavior at elevated pressure and temperature conditions in a membrane contactor. Finite element method using variable element size with smaller elements near the interface was used to solve the equations. In this study, SPG glass membrane with a pore size of 100 nms and porosity of 0.56 was chosen as the base membrane material due to the good thermal stability, high porosity and sharp pore size distribution. In the simulation, the effects of membrane configurations (e.g. membrane diameters, length, thickness, porosity and pore size) on the CO<sub>2</sub> removal efficiency were studied. In terms of the absorbent, 1-Butyl-3-methylimidazolium bis(trifluoromethanesulfonyl)imide [Bmim][Tf<sub>2</sub>N] was chosen as the base ionic liquid absorbent due to the superior thermal stability, relatively low viscosity and high CO<sub>2</sub> absorption capacity. The effects of absorbent ionic liquid properties (e.g. Henry's law constant, viscosity etc.) were also studied. Furthermore, the effects of operation parameters (e.g. liquid flow rate, gas flow rate etc.) on the CO<sub>2</sub> removal efficiency were systematically investigated.

## 2. Model development

In the present study, a numerical analysis of CO<sub>2</sub> separation from syngas in a tubular membrane contactor is conducted by means of deriving and solving the continuity equations, including three domains: the gas, porous membrane, and absorbent sections. As shown in Fig. 2, the gas phase is fed from the shell side, and the liquid phase is fed counter-currently from the core side. Unless mentioned, the membrane contactor is considered to be operated under non-wetted condition, which means only the gas phase diffuses in the membrane.

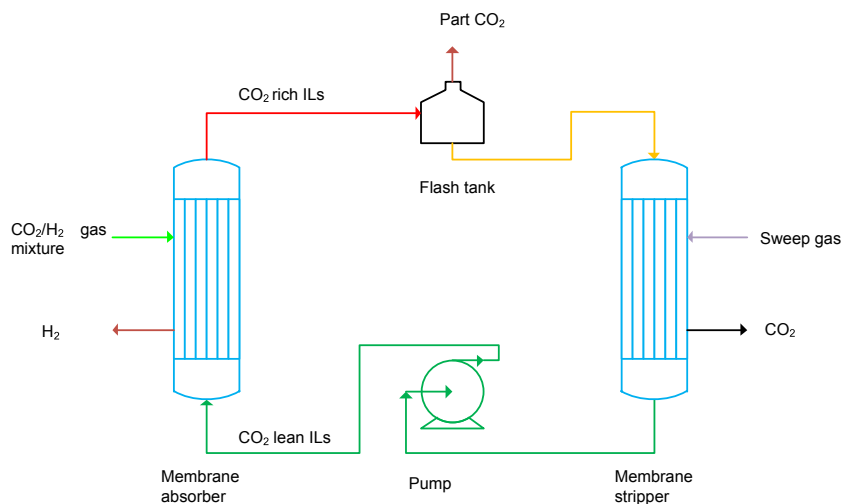


Fig. 1. Schematic representative of the novel membrane contactor for pre-combustion CO<sub>2</sub> capture [21].

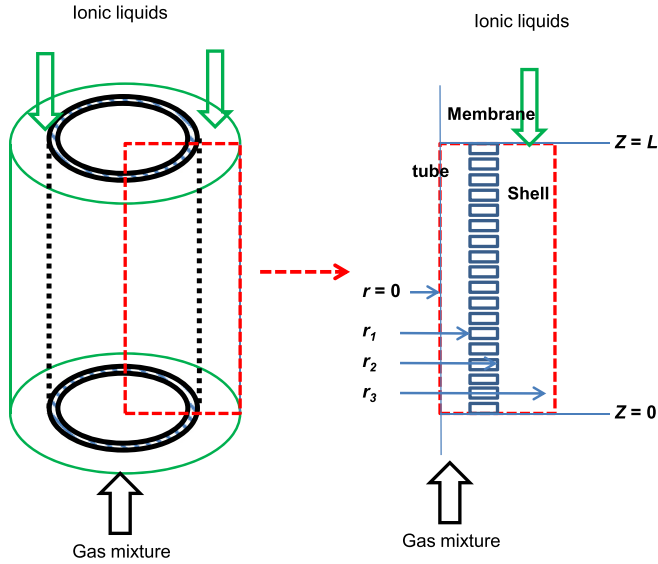


Fig. 2. Schematic diagram of the membrane contactor and section used in the model equations.

### 2.1. Assumptions

To simplify the problem, there are some assumptions for this process:

- Membrane contactor operated in countercurrent mode, gas in the tube and liquid in the shell side;
- Steady state and isothermal process;
- Concentration gradient in both radial and axial directions;
- Membrane acts as a non-selective barrier;
- Ionic liquids serve as physical absorbent (no chemical reaction considered);
- Laminar flow conditions.

### 2.2. Mass transfer equations

#### 2.2.1. Shell side

Based on the above assumptions, the concentration equation for transport of  $\text{CO}_2$  in the shell side for steady-state condition could be expressed as below:

$$D_{\text{CO}_2\text{-shell}} \left[ \frac{\partial^2 C_{\text{CO}_2\text{-shell}}}{\partial r^2} + \frac{1}{r} \frac{\partial C_{\text{CO}_2\text{-shell}}}{\partial r} + \frac{\partial^2 C_{\text{CO}_2\text{-shell}}}{\partial z^2} \right] = V_{\text{CO}_2\text{-shell}} \frac{\partial C_{\text{CO}_2\text{-shell}}}{\partial z} \quad (1)$$

where  $D_{\text{CO}_2\text{-shell}}$ ,  $C_{\text{CO}_2\text{-shell}}$  and  $V_{\text{CO}_2\text{-shell}}$  denote the  $\text{CO}_2$  diffusivity,  $\text{CO}_2$  concentration and liquid velocity in the axial direction in the shell side, respectively.

Gas diffusion coefficient in ionic liquids can be described by equation (2) [45]:

$$D_{\text{CO}_2} = 6.7 \cdot 10^5 \cdot \mu^{-0.66} \cdot M_{\text{IL}}^{-0.89} \cdot \rho_{\text{IL}}^{4.8} \cdot \frac{1}{T^{3.3}} \quad (2)$$

In which  $D_{\text{CO}_2}$  is  $\text{CO}_2$  diffusion coefficient in ionic liquids ( $\text{cm}^2/\text{s}$ ),  $\mu$  is the viscosity of ionic liquids ( $\text{mPa}\cdot\text{s}$ ),  $M_{\text{IL}}$  is the molecular weight of ionic liquid ( $\text{g}/\text{mol}$ ),  $\rho_{\text{IL}}$  is the density of the ionic liquids ( $\text{g}/\text{cm}^3$ ),  $T$  is temperature (K).

According to [46,47], both ILs viscosity and density are temperature dependent and can be expressed as equations (3) and (4), respectively [47]:

$$\rho_{\text{IL}} = (1.72 - 9.4 \cdot 10^{-3} \cdot T) \cdot 1000 \quad (3)$$

Temperature dependency of density [46]:

$$\mu = 1.25 \cdot \exp\left(\frac{625}{T - 180}\right) \quad (4)$$

The velocity profile in the shell side can be characterized by Happel's model as shown in equation (5) [48]:

$$V_{z\text{-shell}} = 2u \left[ 1 - \left(\frac{r_2}{r_3}\right)^2 \right] \cdot \frac{(r/r_3)^2 - (r_2/r_3)^2 + 2 \ln(r_2/r)}{3 + (r_2/r_3)^4 - 4(r_2/r_3)^2 + 4 \ln(r_2/r_3)} \quad (5)$$

where  $u$ ,  $r_3$ ,  $r_2$ , refers to the average velocity, the radius of free surface and the outer radius of fiber, respectively. In which  $r_3$  can be expressed as shown in equation (6):

$$r_3 = \left(\frac{1}{1 - \Theta}\right)^{1/2} \cdot r_2 \quad (6)$$

where  $\Theta$  is the volume fraction of the membrane in the module:

$$1 - \Theta = \frac{nr_2^2}{R^2} \quad (7)$$

$n$  is the number of fibers and  $R$  is the module inner radius. To our case, there is only one membrane in the membrane module, thus  $n = 1$  and  $r_3 = R$ .

The initial and boundary conditions for equation (1) can be expressed in Table 1:

Temperature dependency of Henry constant of the ionic liquids [49]:

$$H_{\text{Px}} = \exp\left(5.006 + 8.455 \cdot 10^2 \cdot \frac{1}{T} - 3.863 \cdot 10^5 \cdot \frac{1}{T^2}\right) \quad (8)$$

$m$  is the distribution factor of the concentration of  $\text{CO}_2$  in gas phase and liquid phase and can be calculated from the following equation [50]:

Table 1  
Initial and boundary conditions at shell side.

Position	Boundary conditions	Description
$z = L$	$C_{\text{CO}_2\text{-shell}} = 0$	Inlet boundary
$r = r_3$	$\frac{\partial C_{\text{CO}_2\text{-shell}}}{\partial r} = 0$	Symmetry boundary
$r = r_2$	$C_{\text{CO}_2\text{-shell}} = m \cdot C_{\text{CO}_2\text{-membrane}}$	Porous membrane

$$m = \frac{\rho_{IL} * R_g * T_*}{M_{IL}} * \frac{1}{k_{px}} * \frac{1}{101.325} \quad (9)$$

### 2.2.2. Membrane phase

The concentration equation for mass transfer of CO<sub>2</sub> in the membrane is considered to be due to the gas diffusion:

$$D_{CO_2-membrane} \left[ \frac{\partial^2 C_{CO_2-membrane}}{\partial r^2} + \frac{1}{r} \frac{\partial C_{CO_2-membrane}}{\partial r} + \frac{\partial^2 C_{CO_2-membrane}}{\partial z^2} \right] = 0 \quad (10)$$

where  $D_{CO_2-membrane}$  and  $C_{CO_2-membrane}$  are the diffusion coefficient and the concentration of CO<sub>2</sub> across the membrane, respectively.

In our study, porous membrane is used thus the effective gas diffusivity in the membrane is:

$$D_m = D_g * \frac{\varepsilon}{\tau} \quad (11)$$

where  $\varepsilon$  and  $\tau$  are the porosity and tortuosity of the porous membrane, respectively. And the  $\tau$  can be estimated from  $\varepsilon$  as shown in equation (12):

$$\tau = \frac{(2 - \varepsilon)^2}{\varepsilon} \quad (12)$$

Boundary conditions for equation (10) are listed in Table 2:

### 2.2.3. Tube side

The differential mass-transfer balance for CO<sub>2</sub> transport in the shell is given in the follow equation:

$$D_{CO_2-tube} \left[ \frac{\partial^2 C_{CO_2-tube}}{\partial r^2} + \frac{1}{r} \frac{\partial C_{CO_2-tube}}{\partial r} + \frac{\partial^2 C_{CO_2-tube}}{\partial z^2} \right] = V_{CO_2-tube} \frac{\partial C_{CO_2-tube}}{\partial z} \quad (13)$$

where  $D_{CO_2-tube}$ ,  $C_{CO_2-tube}$  and  $V_{CO_2-tube}$  denote the CO<sub>2</sub> diffusivity, concentration and liquid velocity in the axial direction in the tube side, respectively.

The diffusion coefficient in gas side can be estimated by equation (14) [56]:

$$D_{CO_2} = \frac{4.36 * 10^{-5} * T_g^{3/2} * \sqrt{\frac{1}{M_a} + \frac{1}{M_b}}}{P * (v_a^{1/3} + v_b^{1/3})} \quad (14)$$

Table 2  
Boundary conditions for equation (10).

Position	Boundary conditions	Description
$r = r_1$	$C_{CO_2-tube} = C_{CO_2-membrane}$	Porous membrane
$r = r_2$	$C_{CO_2-membrane} = C_{CO_2-shell}/m$	

where  $D_{CO_2}$  is the CO<sub>2</sub> diffusion coefficient in gas phase, the  $M_a$  and  $M_b$  are the molecular weight of the two gases, for our case, they are CO<sub>2</sub> and Helium;  $P$  is the absolute gas pressure(atm);  $v_a$  and  $v_b$  is molar volumes at the normal boiling point for gas A and B respectively.

Velocity profile inside the tube is assumed to follow Newtonian laminar flow:

$$V_{z-tube} = 2u \left[ 1 - \left( \frac{r}{r_1} \right)^2 \right] \quad (15)$$

where  $u$  represents the average velocity in the tube side.

The initial and boundary conditions for equation (13) are listed in Table 3.

### 2.3. Design basis and solution

The specifications of the membrane module are listed in Table 4.

The above model equations for the tube, membrane and shell sides with the appropriate boundary conditions and physical properties were solved using COMSOL Multiphysics software. The finite difference element method is used for numerical solution of the PDE equations (equation (1), (10), and (13)). A Dell laptop with the characteristics of RAM 8.00 GB and Intel Core i5-3320M CPU at 2.60 GHz and 64-bit operating system was used to solve the coupled partial differential equations.

## 3. Results and discussion

Concentration profile of CO<sub>2</sub> along the membrane radial direction, tube side is used to characterize the CO<sub>2</sub> removal of the membrane contactor. Unless mentioned, the basic operation conditions are as follows:  $u_{gas} = 4.2$  mm/s,  $u_{liquid} = 6.9$  mm/s,  $T = 353$  K, Membrane length = 300 mm,

Table 3  
Initial and boundary conditions for equation (13).

Position	Boundary conditions	Description
$z = 0$	$C_{CO_2-tube} = C_0$	Inlet boundary
$r = 0$	$\frac{\partial C_{CO_2-tube}}{\partial r} = 0$	Symmetry boundary
$r = r_1$	$C_{CO_2-tube} = C_{CO_2-membrane}$	Porous membrane

Table 4  
Specifications of the membrane module.

Parameter	Value
Inner radius of tube, $r_1$	5 mm
Outer radius of tube, $r_2$	5.2 mm
Membrane thickness, $\delta_m$	0.2 mm
Inner radius of membrane module, $r_3$	6.5 mm
Length of contactor, $L$	300 mm
Porosity of membrane, $\varepsilon_m$	0.56
Membrane tortuosity, $\tau_m$	3.7
Operation pressure, $P$	20 bar
CO <sub>2</sub> concentration in feed (volume)	45%
Ionic liquid	[Bmim][Tf <sub>2</sub> N]

Membrane diameter = 5 mm, Membrane thickness = 0.2 mm,  
Wetting ratio = 0, Porosity = 0.56.

### 3.1. Mass transfer coefficients

Gas side mass transfer coefficient can be expressed as shown in equation (16) [51]:

$$k_g = 1.25 * \left(\frac{\vartheta}{D_g}\right)^{1/3} * \left(\frac{d_h^2 * v_g}{L * \vartheta}\right)^{0.93} * \frac{D_g}{d_h} \quad (16)$$

where  $v_g$  is the kinematic viscosity ( $\text{m}^2 \text{s}^{-1}$ ) and can be expressed as  $v_g = \frac{\mu_g}{\rho_g}$ ,  $\mu_g$  is the dynamic viscosity of the gas (Pa s or  $\text{N s m}^{-2}$  or  $\text{kg m}^{-1} \text{s}^{-1}$ ) and  $\rho_g$  is the density of the gas ( $\text{kg m}^{-3}$ ).  $d_h$  is the hydraulic diameter (m),  $v_g$  represents the gas velocity ( $\text{m s}^{-1}$ ),  $L$  denotes the length of the membrane (m), and  $D_{g,b}$  is the bulk gas diffusivity ( $\text{m}^2 \text{s}^{-1}$ ), which can be calculated from equation (14).

Under un-wetted conditions, the membrane side mass transfer coefficient can be expressed as:

$$k_m = \frac{D_g * \varepsilon_m}{\delta_m * \tau_m} \quad (17)$$

In which the  $\varepsilon_m$ ,  $\delta_m$  and  $\tau_m$  are the membrane porosity, thickness and tortuosity.

When partial wetting of the membrane occurs, the equation for  $k_m$  can change to:

$$k_m = \frac{D_{eff} * \varepsilon_m}{\delta_m * \tau_m} \quad (18)$$

where the  $D_{eff}$  is the effective diffusivity in the membrane, which can be expressed as: effective diffusivity in the membrane

$$D_{m-eff} = \left(\frac{1}{\frac{1-\phi}{D_g} + \frac{\phi}{D_l}}\right) * \frac{\varepsilon}{\tau} \quad (19)$$

In which the  $\phi$  is the membrane pore wetting ratio.

Liquid side mass transfer coefficient ( $k_l$ ) can be predicted by the following equation:

$$Sh \propto f(\phi^*) * \left(\frac{d}{L}\right)^\alpha * Re^\beta * Sc^\gamma \quad (20)$$

where the  $\phi^*$  is packing density,  $\alpha$ ,  $\beta$  and  $\gamma$  are constants,  $Sc$  is the Schmidt number; and  $Re$  is the Reynolds number. According to our operation conditions (e.g., the packing density, the  $Re$  number value), the equation (20) can be expressed as [52]:

$$Sh = 0.09 * (1 - \phi^*) * Re^{(0.48+0.16\phi^*)} * Sc^{0.33} \quad (21)$$

According to the operation conditions, these three mass transfer coefficients were calculated and shown in Fig. 3. Similar to most of the membrane contactors applying for  $\text{CO}_2$  separation, it is clearly shown in Fig. 3, the mass transfer coefficient in the liquid phase is two magnitudes lower than the mass transfer coefficient in gas and membrane phase, demonstrating the mass transfer resistance relies on the liquid

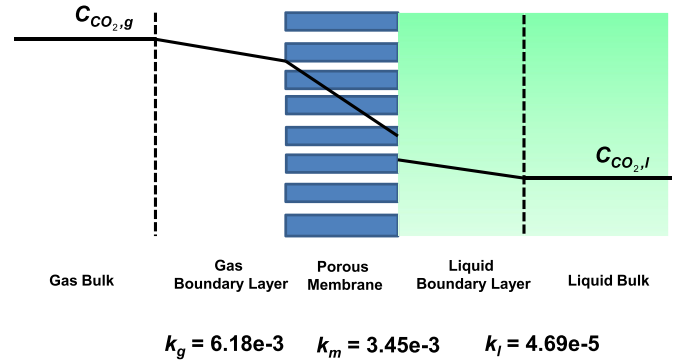


Fig. 3. Mass transfer coefficient in gas, membrane and liquid phase.

phase. It is worth mentioning that in un-wetted condition, the mass transfer coefficient in membrane phase only slightly lower than the mass transfer coefficient in the gas phase. Hence the key point to achieve high mass transfer rate in the membrane contactor is to improve the mass transfer coefficient in the liquid phase, while at the same time maintain the membrane to be un-wetted.

### 3.2. Influence of membrane configurations

It is commonly accepted the membrane configuration has significant impact on the membrane contactor separation performances. In this section, the effects of different membrane configurations on the membrane contactor separation performances were systematically investigated, including membrane diameter, porosity, thickness as well as membrane length.

#### 3.2.1. Effect of membrane diameter

In this study, the membrane module dimension and the membrane number is fixed, and the gas and liquid velocities are also kept constant. In this case reducing the membrane diameter means the reduction in gas volume flow and the increase in the liquid volume flow, which will enhance the  $\text{CO}_2$  absorption as shown in Fig. 4. As the membrane diameter reduces from 5 mm to 1 mm, the  $\text{CO}_2$  separation concentration

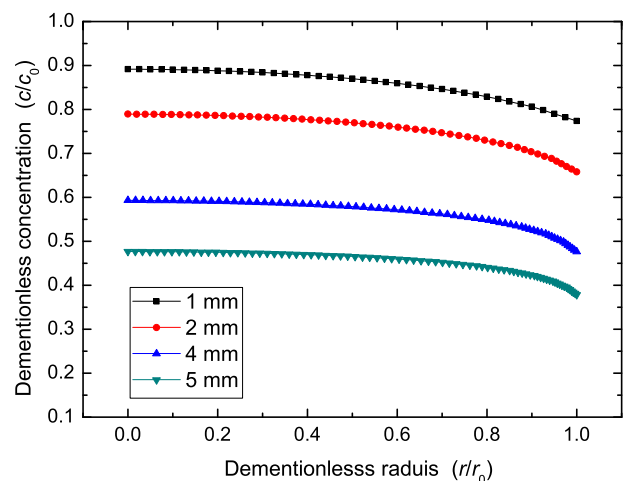


Fig. 4. Effect of membrane diameter on  $\text{CO}_2$  separation performance.

at the outlet of the membrane module greatly reduced. Therefore, it is reasonable to state that reduce the membrane diameter can effectively enhance separation efficiency. In practical applications, hollow fiber membranes with diameter of lower than 1 mm is normally used and better separation performances can be expected.

### 3.2.2. Effect of membrane thickness

Fig. 5 presents the effect of membrane thickness on the CO<sub>2</sub> absorption performances. It is obvious that reducing the membrane thickness can effectively reduce the mass transfer resistance in membrane phase. When the membrane thickness reduced from 0.4 mm to 0.02 mm, the CO<sub>2</sub> outlet concentration can be effectively influenced and has a sharp reduction, and the trend clearly shows the thinner the membrane, the better separation performances. However, in practical applications, the mechanical strength and long-term stability of the membrane should be also taken into consideration when trying to reduce the membrane thickness.

### 3.2.3. Effect of membrane porosity

Influence of membrane porosity on the CO<sub>2</sub> removal efficiency is shown in Fig. 6. According to equation (11), it is clear that higher porosity will reduce the mass transfer resistance in the membrane phase. At the same time, as shown in equation (12), a higher porosity will also lead to a lower tortuosity, and consequently higher gas diffusivity and lower membrane transfer resistance. It can be seen in Fig. 6, increasing porosity from 0.1 to 0.9 (porosity of 0.9 is quite challenging for practical membranes, the number used here is to show the trend of the results), the CO<sub>2</sub> outlet concentration has a deduction of around 40%. Furthermore, at higher membrane porosity, the concentration gradient over the membrane diameter is much smaller, clearly show the mass transfer resistance reduced with porosity increasing in the membrane. In practical applications, there will be a limitation on the maximum porosity for a membrane, due to the difficulties of fabricating high porosity membranes and the challenge of mechanical strength problem.

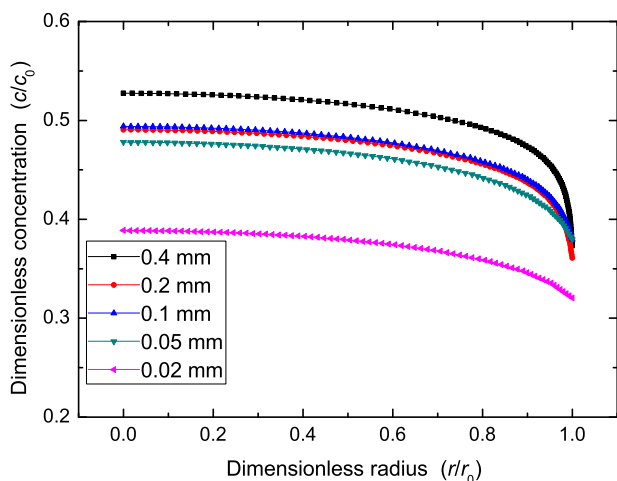


Fig. 5. Effect of membrane thickness on CO<sub>2</sub> separation performance.

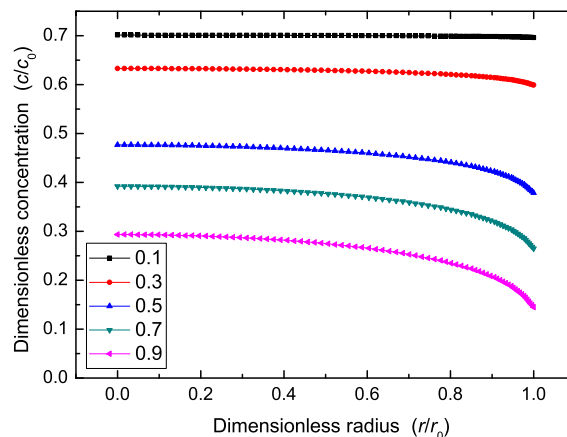


Fig. 6. Effect of membrane porosity on CO<sub>2</sub> separation performance.

### 3.2.4. Effect of membrane length

It is obvious that increments of membrane module length can enhance the CO<sub>2</sub> removal in Fig. 7. The increment of the membrane length resulted in increasing the membrane surface area and the residence time of ILs in the membrane module, which is conducive to the absorption. However, it is well-known that CO<sub>2</sub> concentration in the gas phase drops with membrane module length, resulted in a reduction of mass-transfer driving force and the mass transfer efficiency, thus in practical applications, the membrane module should be optimized to obtain the desired separation targets while keep both capital and operating cost as low as possible. It is worth mentioning, in this study, the pressure drop in the liquid phase was not taken into account. However, in experimental test, the relatively high viscosity will cause significant pressure drop along the membrane module and this pressure drop should always be considered. A long membrane module may result in a pressure drop big enough to surpass the critical entry pressure of the membrane, thus cause membrane wetting and reduce the separation efficiency.

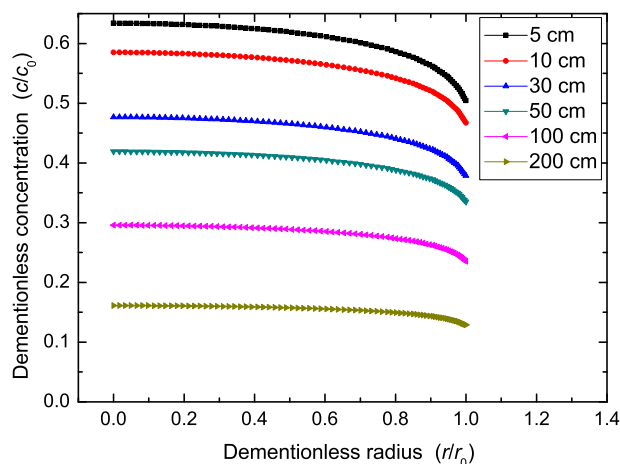


Fig. 7. Effect of membrane length on CO<sub>2</sub> separation performance.

### 3.3. Influence of liquid properties

Liquid properties is one of the key issues need to be considered in the MC processes, as the Henry constant (gas solubility) and the viscosity of the absorbent will have significant influence on the separation performance, thus in this section, the effect of Henry constant and the viscosity have been investigated.

#### 3.3.1. Effect of Henry constant

Absorbents with higher CO<sub>2</sub> solubility (lower Henry constant) will in general result in a better separation performance. As shown in Fig. 8, increasing the Henry constant from 10 bar to 40 bar could reduce the CO<sub>2</sub> concentration at the outlet for approximately 15%. Further reducing the Henry constant (increasing CO<sub>2</sub> solubility) can logically result in higher CO<sub>2</sub> removal efficiency. Employing chemisorption ILs which can chemically react with CO<sub>2</sub> and promote CO<sub>2</sub> absorption can be an option. But it should be pointed out that the viscosity of chemisorption ILs will increase dramatically after absorbed CO<sub>2</sub> [53], consequently the CO<sub>2</sub> diffusivity will be negatively affected.

#### 3.3.2. Influence of viscosity

The effect of viscosity on CO<sub>2</sub> removal is displayed in Fig. 9. As shown in equation (2), the viscosity has huge effect on the gas diffusivity in the liquid side. A higher viscosity results in a lower gas diffusivity coefficient and consequently higher liquid side mass transfer resistance. As shown in Fig. 9, as viscosity of the ILs increased from 5 cP to 500 cP, the CO<sub>2</sub> concentration at the outlet increased more than 10%. It is worth noting that the CO<sub>2</sub> removal efficiency is more sensitive at lower viscosity regime. For example, viscosity changed from 5 cP to 9.27 cP leads to an approximately 4% difference in CO<sub>2</sub> removal, but increasing viscosity from 200 cP to 500 cP only leads to a CO<sub>2</sub> removal difference of about 2%. Furthermore, compared to the ILs with lower viscosity, the concentration gradient over the membrane diameter is bigger

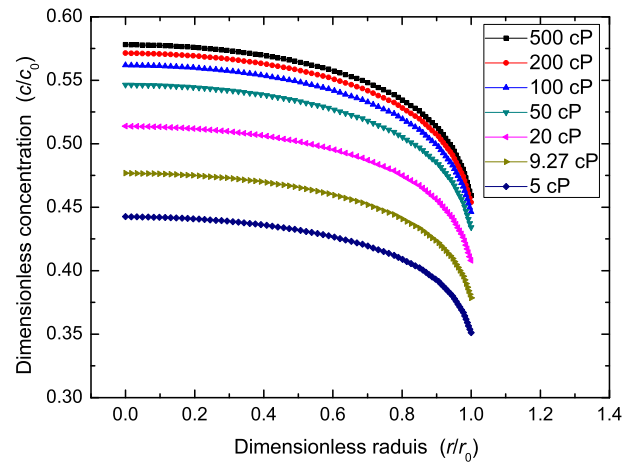


Fig. 9. Influence of viscosity on CO<sub>2</sub> separation performance.

for ILs with higher viscosity, which is consistent with the fact that CO<sub>2</sub> diffusivity is lower in ILs with higher viscosity. Again, in our study, the pressure drop along the membrane module is not considered, otherwise the high viscosity of the liquid will cause significant pressure drop and possible bubbling or membrane wetting.

### 3.4. Influence of operation parameters

As shown in the equations (16) and (20), the mass transfer coefficient of gas phase and liquid phase are function of the gas flow rate and liquid flow rate. At the same time, changing operational temperature can also impact the physical properties of the liquid phase viscosity (e.g. viscosity, density), results in a change in gas diffusivity in liquid phase and consequently the mass transfer coefficient in liquid phase. Therefore, in this section, the effects of different operational parameters on CO<sub>2</sub> removal efficiency were investigated.

#### 3.4.1. Effect of liquid and gas flow rates

As can be seen from Fig. 10, it is reasonable that a small gas flow rate (GFR) provides a better CO<sub>2</sub> removal from the

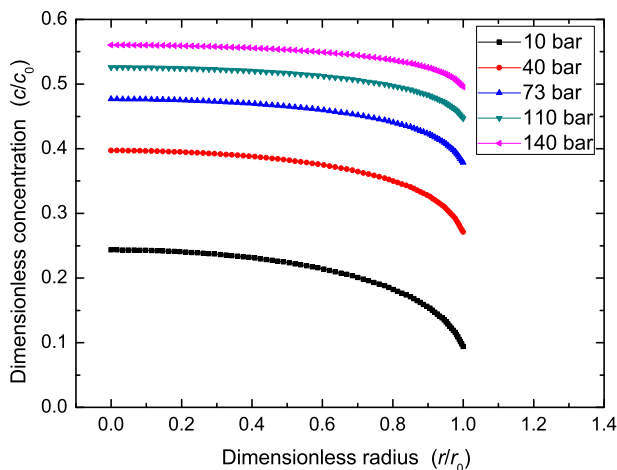


Fig. 8. Influence of Henry's law constant (CO<sub>2</sub> solubility) on CO<sub>2</sub> separation performance.

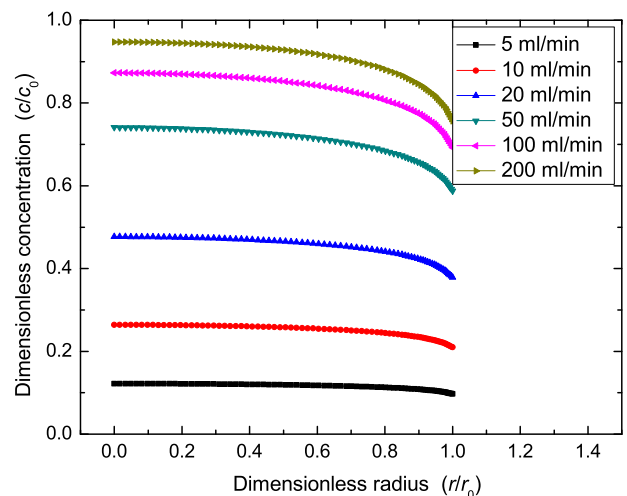


Fig. 10. Effect of gas flow rates on CO<sub>2</sub> separation performance.

gas-phase mixture. Larger GFR leads to higher velocity of the gas phase and thus smaller residual time in the membrane contactor, hence, CO<sub>2</sub> concentration levels at the outlet increase. It is worth mentioning that even the residual CO<sub>2</sub> concentration is higher at high gas phase velocity, the CO<sub>2</sub> flux across the membrane is always increasing with CO<sub>2</sub> velocity. Meaning increasing gas phase velocity can always enhance the CO<sub>2</sub> transport. However, in practical applications, the gas flow rate should be optimized. A high gas flow rate could result in a high CO<sub>2</sub> flux across the membrane, it may also result in a small stage-cut, which is not favorite in practical application.

As expected, the liquid flow rates also have significant effect on the CO<sub>2</sub> removal efficient (Fig. 11). Increasing liquid flow could effectively enhance the CO<sub>2</sub> removal efficiency. However, it should be noted that a high liquid flow rate means huge amount of absorption liquids and powerful pump, which may lead to both high capital and operational cost. Therefore, in practical applications, the liquid flow rate should be optimized to meet the separation requirements at the same time maintaining the minimum energy and capital cost.

### 3.4.2. Effect of operation temperature

Commonly, it is believed that increasing the liquid phase temperature will hinder the dissolution of gases (reduction of CO<sub>2</sub> solubility in absorbents), which will negatively affect the CO<sub>2</sub> removal efficiency; however, at the same time, increasing temperature will reduce the liquid phase viscosity and promote the gas diffusivity, which is favorites for CO<sub>2</sub> absorption. Hence the effect of operational temperature was investigated in this section.

For [Bmim][Tf<sub>2</sub>N] ionic liquids, the temperature dependency of Henry's law constant ( $H_{px}$ ) can be calculated from as equation (8) [45]:

$$H_{px} = \exp\left(5.006 + 8.455 \cdot 10^2 \cdot \frac{1}{T} - 3.863 \cdot 10^5 \cdot \frac{1}{T^2}\right) \quad (8)$$

The temperature dependency of CO<sub>2</sub> diffusivity in [Bmim][Tf<sub>2</sub>N] can be expressed as equation (2) [54]:

$$D_{CO_2} = 6.7 \cdot 10^5 \cdot \mu^{-0.66} \cdot M_{IL}^{-0.89} \cdot \rho^{4.8} \cdot \frac{1}{T^{3.3}} \quad (2)$$

Furthermore, the temperature dependency of CO<sub>2</sub> diffusivity in gas side can be calculated as shown in equation (14) [55]:

$$D_{CO_2} = \frac{4.36 \cdot 10^{-5} \cdot T_g^{3/2} \cdot \sqrt{\frac{1}{M_a} + \frac{1}{M_b}}}{P \cdot (v_a^{1/3} + v_b^{1/3})} \quad (14)$$

The effects of operational temperature were investigated in a range of 303–393 K and results are shown in Fig. 12. It is clear that the overall effect of operational temperature on CO<sub>2</sub> removal efficiency is negative: a higher residual CO<sub>2</sub> concentration was obtained at a higher temperature. Furthermore, at high temperature condition, the CO<sub>2</sub> concentration gradient over the membrane diameter is smaller, denoting relatively smaller mass transfer resistance in the liquid phase. It can be also found the CO<sub>2</sub> concentration differences over the investigated range is not large, meaning operational temperature has limited overall effect on CO<sub>2</sub> removal efficiency.

### 3.4.3. Effect of membrane wetting ratio

Gradual wetting of porous membranes with liquid is the main concern for long-term operation of CO<sub>2</sub> absorption in membrane contactors [56]. Membrane wetting significantly impacts mass transfer coefficients in the membrane phase, leading to a sharp increase in membrane resistance and a rapid decline of absorption performance [57–59]. Generally, the membrane wetting ratio is defined as the ratio between the liquid occupied pore length and the whole pore length. In other words, 1% wetting ratio means all the pores in the membrane are wetted by 1%. As shown in Fig. 13, a small wetting ratio could lead to huge difference in the CO<sub>2</sub> concentration at the outlet. However, as long as the membrane is wetted, then it is not sensitive to wetting ratio any more. For example, the wetting ratio from 1% to 10% only leads to 10% difference in remove efficiency, and these entire results locate at the low separation regime. Therefore, a key point of keeping membrane contactor separation performances is to avoid membrane

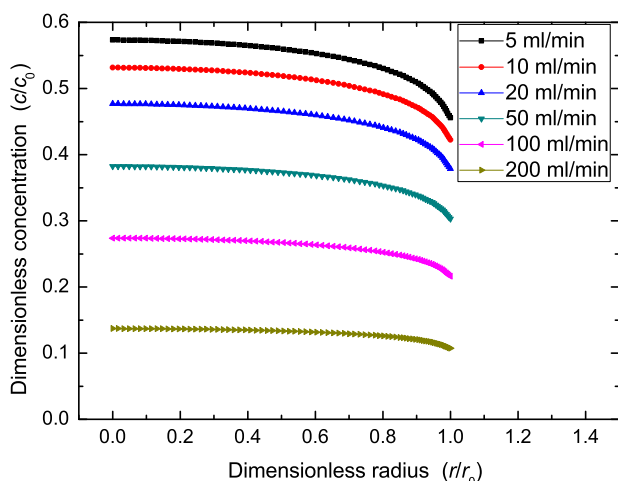


Fig. 11. Effect of liquid flow rates on CO<sub>2</sub> separation performance.

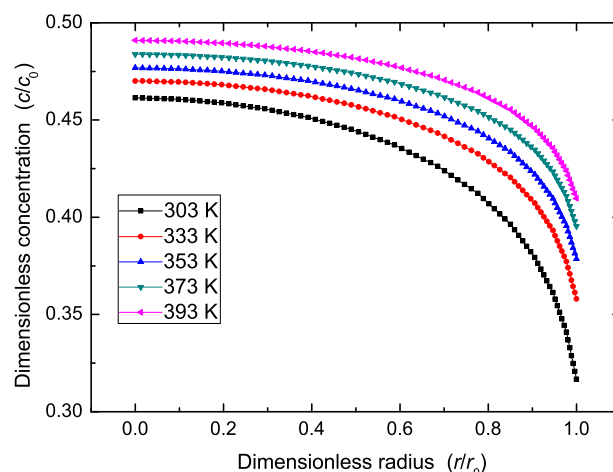


Fig. 12. Effect of operation temperature on CO<sub>2</sub> separation performance.

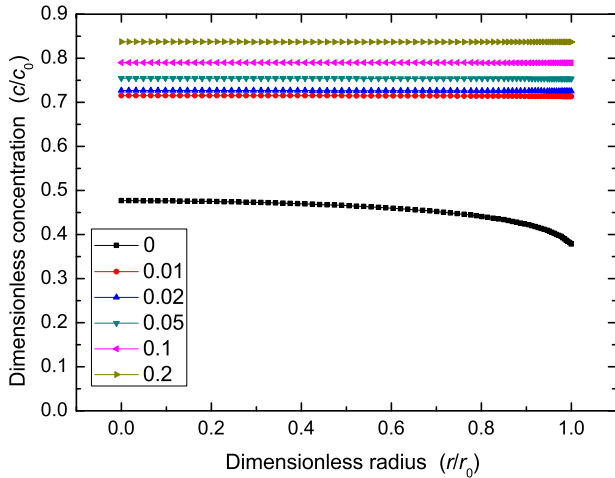


Fig. 13. Effect of membrane wetting ratio on CO<sub>2</sub> separation performance.

wetting. Employing composite membrane with a top dense layer can be one promising option [20,60].

$$D_{m-eff} = \left( \frac{1}{\frac{1-\phi}{D_g} + \frac{\phi}{D_l}} \right) * \frac{\epsilon}{\tau} \quad (19)$$

As the big influence on the membrane wetting ratio, we also calculated the mass transfer coefficient before and after the membrane wetting, as shown in Fig. 13. Even a membrane wetting ratio of 1% dramatically decrease the  $k_m$  for 2 magnitudes (from  $3.45 \times 10^{-3}$  m/s to  $1.53 \times 10^{-5}$  m/s). In other words, the mass transfer resistance increased 2 magnitudes with only 1% membrane was wetted, and the membrane mass transfer resistance is at the same level as the liquid side ( $k_l = 4.69 \times 10^{-5}$  m/s). This result clearly explains why the CO<sub>2</sub> removal efficiency reduces a huge portion with little membrane wetting ratio. Further increase the wetting ratio will slightly change the  $k_m$  at the same magnitude, thus it has only limited effect on the CO<sub>2</sub> removal (as shown in Fig. 14).

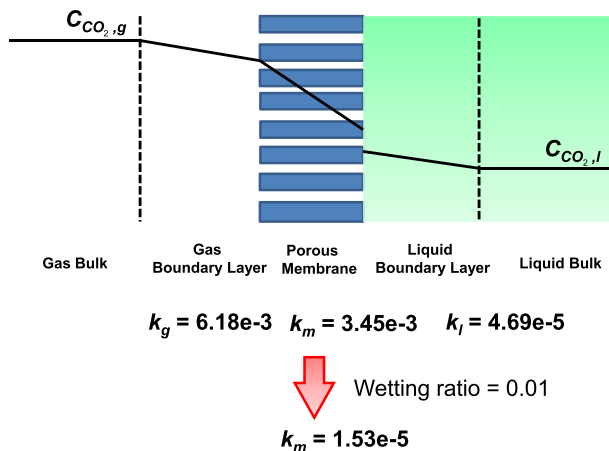


Fig. 14. Influence of membrane wetting ratio on mass transfer coefficient.

### 4. Conclusion

The aim of the present study has been to study the potential of a membrane absorption process for CO<sub>2</sub> capture from syngas at elevated temperature and pressures. A comprehensive 2D mass-transfer model was developed and solved considering non-wetted conditions for a counter-current membrane contactor with ILs as absorbent. The effects of gas liquid parameters (e.g. Henry's law constant, viscosity etc.), membrane configurations (e.g. membrane diameters, thickness, length, porosity etc.), as well as operation parameters (e.g. liquid flow rate, gas flow rate etc.) on the CO<sub>2</sub> removal efficiency were systematically examined and evaluated. Several key findings in this study are listed as follows:

- (1) For a membrane contactor based on physisorption based ionic liquids, the liquid side resistance is about 100 times higher than the gas phase and it is the limiting factor for the CO<sub>2</sub> overall mass transfer;
- (2) The investigation of the effects of membrane configuration shows that increasing membrane length, porosity and reducing membrane thickness promotes CO<sub>2</sub> separation. However, in practical application, other parameters (e.g., membrane mechanical strength, chemical stability) should also be taken into consideration.
- (3) Compared to Henry's law constant, liquid viscosity has relatively small effect on CO<sub>2</sub> absorption.
- (4) Both the gas flow rate and liquid flow rate have large impact on the CO<sub>2</sub> removal efficiency. Compared to gas/liquid flow rate, the operational temperature has limited influence on CO<sub>2</sub> absorption;
- (5) Membrane wetting ratio has significant impact on separation performance. 1% membrane wetting could dramatically increase the membrane resistance and deteriorates CO<sub>2</sub> absorption flux in long-term operation.

According to the simulation results, by proper optimization of operation conditions and absorbent/membrane properties, the ionic liquid based membrane contactors can be a promising alternatives for pre-combustion CO<sub>2</sub> capture at elevated temperature and pressures.

### Conflict of interest

The authors declare that there is no conflict of interest regarding the publication of this paper.

### Acknowledgments

This work is partly supported by the Research Council of Norway through CLIMIT program (MCIL-CO<sub>2</sub> project, 215732).

### Nomenclature

- D* CO<sub>2</sub> diffusivity (cm<sup>2</sup>/s)
- C* CO<sub>2</sub> concentration (mol/L)

$V$	liquid velocity (mm/s)
$M_i$	molecular weight (g/mol)
$T$	temperature (K)
$u$	average velocity (mm/s)
$r_1$	inner radius of membrane (mm)
$r_2$	outer radius of membrane (mm)
$r_3$	radius of free surface (mm)
$n$	number of membrane fibers
$H_{px}$	Henry constant (bar)
$m$	Distribution factor of the concentration of CO <sub>2</sub> in gas phase and liquid phase
$R_g$	gas constant
$P$	pressure (atm)
$L$	membrane length (mm)
$k_g$	gas side mass transfer coefficient (m/s)
$k_m$	membrane side mass transfer coefficient (m/s)
$D_{eff}$	effective diffusivity in the membrane (m <sup>2</sup> /s)
$d_h$	hydraulic diameter (mm)
$z$	cylindrical coordinate (mm)

#### Greek letter

$\mu$	viscosity (mPa*s)
$\phi$	membrane pore wetting ratio
$\phi^*$	membrane packing density
$\vartheta_i$	molar volumes at the normal boiling point (mol/ml)
$\delta$	membrane thickness (mm)
$\varepsilon$	membrane porosity
$\tau$	membrane tortuosity
$\Theta$	volume fraction of the membrane in the module
$\rho_{IL}$	density of the ionic liquids (g/cm <sup>3</sup> )

#### References

- [1] M.E. Boot-Handford, et al., *Energy & Environ. Sci.* 7 (1) (2014) 130–189.
- [2] J.D. Figueroa, et al., *Int. J. Greenh. Gas Control* 2 (1) (2008) 9–20.
- [3] C. Descamps, C. Bouallou, M. Kanniche, *Energy* 33 (6) (2008) 874–881.
- [4] S. Smart, et al., *Energy Environ. Sci.* 3 (3) (2010) 268–278.
- [5] X.M. Jie, et al., *Ind. Eng. Chem. Res.* 53 (8) (2014) 3305–3320.
- [6] A. Mansourizadeh, A.F. Ismail, *J. Hazard. Mater.* 171 (1–3) (2009) 38–53.
- [7] S. Zhao, et al., *J. Membr. Sci.* 511 (2016) 180–206.
- [8] Z.E. Zhang, et al., *Glob. Nest J.* 16 (2) (2014) 354–373.
- [9] Z. Wang, et al., *Ind. Eng. Chem. Res.* 52 (34) (2013) 12170–12182.
- [10] N. Boucif, et al., *AIChE J.* 58 (9) (2012) 2843–2855.
- [11] J.G. Lu, et al., *Energy Fuels* 24 (2010) 4617–4626.
- [12] W.F. Zhang, Z.H. Lin (Iceesd 2011), Pts 1–5, *Prog. Environ. Sci. Eng.* 356–360 (2012) 1362–1366.
- [13] S. Masoumi, et al., *Energy Fuels* 27 (9) (2013) 5423–5432.
- [14] M. Mehdipour, et al., *Energy Fuels* 27 (4) (2013) 2185–2193.
- [15] L.H. Cheng, et al., *J. Membr. Sci.* 324 (1–2) (2008) 33–43.
- [16] C. Makhoulfi, et al., *J. Membr. Sci.* 455 (2014) 236–246.
- [17] X. Jie, et al., *Ind. Eng. Chem. Res.* 52 (26) (2013) 8783–8799.
- [18] P. Luis, A. Garea, A. Irabien, *J. Membr. Sci.* 330 (1) (2009) 80–89.
- [19] J. Albo, P. Luis, A. Irabien, *Ind. Eng. Chem. Res.* 49 (21) (2010) 11045–11051.
- [20] Z. Dai, L. Ansaloni, L. Deng, *Ind. Eng. Chem. Res.* 55 (20) (2016) 5983–5992.
- [21] Z. Dai, L. Deng, *Int. J. Greenh. Gas Control* 54 (2016) 59–69.
- [22] J. Albo, A. Irabien, *J. Chem. Technol. Biotechnol.* 87 (10) (2012) 1502–1507.
- [23] J. Albo, P. Luis, A. Irabien, *Desalination Water Treat.* 27 (1–3) (2011) 54–59.
- [24] S.J. Zhang, et al., *Chem. Soc. Rev.* 43 (22) (2014) 7838–7869.
- [25] M.A. Malik, M.A. Hashim, F. Nabi, *Chem. Eng. J.* 171 (1) (2011) 242–254.
- [26] E. Santos, J. Albo, A. Irabien, *J. Membr. Sci.* 452 (2014) 277–283.
- [27] J. Albo, T. Tsuru, *Ind. Eng. Chem. Res.* 53 (19) (2014) 8045–8056.
- [28] J. Deng, et al., *RSC Adv.* 6 (51) (2016) 45184–45192.
- [29] Z. Dai, et al., *Sci. China Chem.* 59 (5) (2016) 538–546.
- [30] Z. Dai, et al., *J. Membr. Sci.* 523 (2017) 551–560.
- [31] Z. Dai, L. Ansaloni, L. Deng, 2, *Green Energy Environ.* (2016) 1–27.
- [32] J. Wang, et al., *Green Energy Environ.* 1 (1) (2016) 43–61.
- [33] J. Chau, et al., *J. Membr. Sci.* 453 (2014) 61–70.
- [34] K.A. Hoff, H.F. Svendsen, *Chem. Eng. Sci.* 116 (2014) 331–341.
- [35] M. Saidi, et al., *J. Nat. Gas Sci. Eng.* 18 (2014) 274–285.
- [36] S.M.R. Razavi, et al., *Int. J. Greenh. Gas Control* 15 (2013) 142–149.
- [37] S. Boributh, et al., *J. Membr. Sci.* 401 (2012) 175–189.
- [38] S. Boributh, et al., *J. Membr. Sci.* 380 (1–2) (2011) 21–33.
- [39] S. Boributh, et al., *J. Membr. Sci.* 372 (1–2) (2011) 75–86.
- [40] S. Shirazian, S.N. Ashrafizadeh, *Sep. Sci. Technol.* 45 (4) (2010) 515–524.
- [41] M. Rezakazemi, et al., *Chem. Eng. J.* 168 (3) (2011) 1217–1226.
- [42] R. Faiz, M. Al-Marzouqi, *J. Membr. Sci.* 365 (1–2) (2010) 232–241.
- [43] Z.E. Zhang, et al., *Industrial Eng. Chem. Res.* 53 (36) (2014) 14075–14083.
- [44] Y.F. Yan, et al., *Energy Fuels* 28 (9) (2014) 5745–5755.
- [45] J. Jacquemin, et al., *J. Solut. Chem.* 36 (8) (2007) 967–979.
- [46] K.R. Harris, M. Kanakubo, L.A. Woolf, *J. Chem. Eng. Data* 53 (5) (2008) 1230.
- [47] K.R. Harris, M. Kanakubo, L.A. Woolf, *J. Chem. Eng. Data* 52 (6) (2007) 2425–2430.
- [48] J. Happel, *Aiche J.* 5 (2) (1959) 174–177.
- [49] Z.G. Lei, C.N. Dai, B.H. Chen, *Chem. Rev.* 114 (2) (2014) 1289–1326.
- [50] R. Sander, *Compilation of Henry's law constants for inorganic and organic species of potential importance in environmental chemistry*, 1999.
- [51] A. Gabelman, S.-T. Hwang, *J. Membr. Sci.* 159 (1–2) (1999) 61–106.
- [52] J.M. Zheng, Y.Y. Xu, Z.K. Xu, *Sep. Sci. Technol.* 38 (6) (2003) 1247–1267.
- [53] K.E. Gutowski, E.J. Maginn, *J. Am. Chem. Soc.* 130 (44) (2008) 14690–14704.
- [54] Y. Hou, R.E. Baltus, *Ind. Eng. Chem. Res.* 46 (24) (2007) 8166–8175.
- [55] E.R. Gilliland, *Ind. Eng. Chem.* 26 (6) (1934) 681–685.
- [56] S. Mosadegh-Sedghi, et al., *J. Membr. Sci.* 452 (2014) 332–353.
- [57] H. Kreulen, et al., *J. Membr. Sci.* 78 (3) (1993) 197–216.
- [58] H. Kreulen, et al., *J. Membr. Sci.* 78 (3) (1993) 217–238.
- [59] Z. Wang, et al., *Energy Fuels* 27 (11) (2013) 6887–6898.
- [60] C.A. Scholes, et al., *Int. J. Greenh. Gas Control* 42 (2015) 66–74.